JOURNAL OF MATERIALS SCIENCE 39 (2004) 6591–6596

Influence of synthesis methodology and post treatments on structural and textural variations in $MgAlCO_3$ hydrotalcite

S. KANNAN
Silicates and Catalysis Discipline, Central Salt and Marine Chemicals Research Institute, Bhavnagar 364 002, India
E-mail: salt@csir.res.in; kanhemad1@sancharnet.in

MgAl-CO_3 hydrotalcite was synthesized by a new method namely instantaneous precipitation (IP) and compared for structural and textural variations for both fresh and aged samples with the conventionally synthesized coprecipitated (COP) sample. PXRD showed a pattern similar to pure hydrotalcite, irrespective of synthesis methodology used, however, crystallinity and crystallite size was higher for both fresh and aged samples synthesized by IP method than for the corresponding samples synthesized by COP method. Significant variation in the particle morphology was noted, wherein nearly aggregated spherical particles were observed with IP method while elongated hexagonal platelets were observed with COP method. N_2 adsorption measurements showed a Type-IV isotherm for aged samples, however, pore size distribution varied with synthesis methodology. Particle size variations showed, a broad distribution for both fresh and aged samples synthesized by IP method while a size distribution for fresh COP sample changed to a bimodal distribution upon aging with a concomitant increase in average particle size. The difference in the properties of these samples with the variation in synthesis methodology and post treatments may be ascribed for variations in local hydrothermal effects, mixing at both microscopic and macroscopic levels and in degree of supersaturation.

1. Introduction

In our earlier work, we have disclosed microwave assisted rapid synthesis of well crystalline MgM(III) hydrotalcites using a new synthesis methodology known as instantaneous precipitation [1]. It is well known that synthesis methodology and post synthesis treatments have a strong influence on the final properties of the materials. Although synthesis of hydrotalcites under different supersaturation levels are known, detailed fundamental investigations on the variation of physicochemical properties with synthesis methodology is limited [2]. We have extended our study to unravel detailed physicochemical properties of the materials obtained through instantaneous precipitation (IP) method and compared them with the properties obtained through conventional coprecipitation (COP) method. Briefly, hydrotalcite-like (HT-like) compounds are a class of layered materials consisting of positively charged brucite-like layers interspersed with anions and water molecules. An increasing attention has been drawn to these compounds owing to their diverse applications such as catalysts [3–5], supports [6], ion-exchangers [7, 8] and polymer additives [9], however, the nature of application is influenced by optimum physicochemical properties in particular by, crystallinity, surface texture and particle size. Various methods have been reported such as salt-oxide method [10], precipitation at different levels of supersaturation [11], induced hydrolysis [12], reconstruction [13] and anion-exchange [14] to synthesize these compounds with altered physicochemical characteristics. However, coprecipitation at fixed pH is the most commonly used method, usually results in well crystalline materials. In this affiliation, we have earlier synthesized a wide variety of compounds of general formula M(II)M(III)CO_3-HT where M(II) = Mg, Ni, Co, Cu and Zn and M(III) = Al, Fe and Cr using this methodology [15–18]. In this paper, we report the variations in structural and textural properties of $MgAlCO_3$-HT synthesized by two different methods namely instantaneous precipitation (IP) and coprecipitation (COP). Further, to delineate the differences observed upon aging, comparison between corresponding fresh and aged samples were also done.

2. Experimental

2.1. Synthesis of MgAl-hydrotalcites

In a typical synthesis, two solutions namely Solution-A containing 0.06 moles of $Mg(NO_3)_2$ and 0.02 moles

of $Al(NO_3)_3$ in 100 ml water and Solution-B containing 0.2 moles of NaOH and 0.02 moles of Na_2CO_3 in 100 ml water were prepared. In IP method, both solutions were rapidly added (<5 s) to double distilled water (100 ml) under stirring and was continued for 2 min. Experiments were optimized to obtain a final pH around 10. In COP method both solutions were added slowly and simultaneously for 90 min (∼1 ml/min) to 100 ml of double distilled water while maintaining the pH in between 9 and 10. A portion of the sample from both methods was immediately filtered, washed and dried and referred here as *fresh* sample while the remaining portion was subjected to aging at 338 K for 24 h without stirring and referred as *aged* sample. Samples were dried in an air oven at 383 K for 12 h. The samples are denoted here as MgAl-COP and MgAl-IP for samples obtained by coprecipitation and instantaneous precipitation respectively, with a suffix F or A indicating fresh or aged samples.

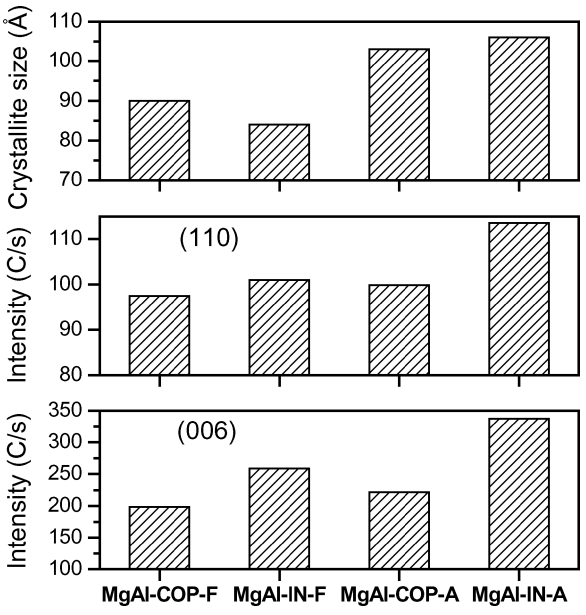

Figure 1 PXRD intensity of (006), (110) reflections and crystallite size of samples synthesized.

2.2. Characterization methods

Powder X-ray diffraction (PXRD) data were recorded in a Philips X'Pert MPD system using Cu K_α radiation ($\lambda = 1.5406$ Å). A step size of 0.14° and a step time of 5.6 s were used for data collection and were processed using PC-APD software. The X-ray beam voltage was 40 kV and beam current was 55 mA. Debye-Scherrer equation ($t = 0.89\lambda/\beta \cos\theta$, where t is crystallite size, β is FWHM and θ is diffraction angle) was employed for calculation of crystallite size after taking into consideration of instrumental line broadening.

Thermogravimetric (TG) analysis was performed in a Perkin-Elmer thermal analyzer (TG-DSC-7) in the temperature range 323–1023 K with a heating rate of 10°C/min under nitrogen atmosphere using 5–10 mg of sample. The evolved gases observed during decomposition were analyzed on-line by a computer-controlled Quadruple mass spectrometer (Balzers Quadstar 421).

In situ FT-IR spectroscopy studies were carried out in a Bruker IFS-66 apparatus at a spectral resolution of 2.0 cm^{-1} accumulating 128 scans. Self-supporting wafers (ca. 10 mg cm^{-2}) were prepared from the sample powders and heated directly in the IR cell. The latter was connected to a vacuum apparatus with a residual pressure less than 10^{-3} P.

Transmission electron microscopy (TEM) was taken in a Jeol electron microscope (Model - 200CX) with an operating voltage of 200 kV. The samples were dispersed in hexane and a drop of supernatant suspension was poured on to a carbon coated copper grid and dried before measurements. Scanning was done at different regions of the samples to confirm homogeneity.

^{27}Al MAS-NMR spectra were recorded at 52.15 MHz in a Bruker (Avance DPX 200) NMR spectrometer using 1 M aluminum nitrate solution as internal standard. The samples were spun at 3000 rpm and recorded at room temperature.

N_2 adsorption measurements were carried out in a sorptometer (ASAP 2010, Micromeritics, USA) at 77 K. Prior to adsorption, samples were degassed at 343 K under vacuum (10^{-2} mbar). Particle size measurements were carried out by wet dispersion technique using water as dispersant in a Malvern Mastersizer-2000 (Model-Hydro2000S) employing laser light scattering. The samples were spun at 2500 rpm for homogenization and 2000 scans were taken for averaging the measurements.

3. Results and discussion

Irrespective of the synthesis methodology used, PXRD showed a pure HT-like phase for both fresh and aged samples without co-forming any additional impurity phases. Fig. 1 shows the variation in intensity of (006) and (110) reflections (these are being chosen to reflect both basal and *ab* plane reflections) of the samples synthesized. From the figure, one can say when comparing the corresponding fresh and aged samples, those synthesized by IP method are more crystalline than COP method. As expected, aging treatment had enhanced the crystallinity, however, the enhancement was higher for IP method. Crystallite size measurements substantiated the above crystallinity variation, although MgAl-COP-F is slightly higher compared to MgAl-IP-F, with MgAl-IP-A exhibiting the maximum size (Fig. 1). Lattice parameters calculated, by indexing the peaks under hexagonal crystal system (Table I), showed a drop in '*a*' parameter (which is the average cation-cation distance in the brucite-like layers) for IP samples compared to COP samples. This is in agreement with the elemental analysis results given in Table I, which showed a lower Mg/Al atomic composition for IP sample (ionic radius of Mg^{2+}-0.72 Å; Al^{3+}-0.53 Å), in other words, lower concentration of magnesium in brucite-like sheets. However, no significant difference in '*c*' parameter was noticed between both fresh and aged samples, irrespective of synthesis methodology employed. ^{27}Al MAS-NMR of these samples showed a sharp peak at δ around 5 ppm confirming the presence of octahedral aluminum. However, long range ordering of the lattice can be assessed from the asymmetric line

TABLE I Physicochemical properties of fresh and aged samples synthesized by IP and COP methods

	IP method		COP method	
	Fresh	Aged	Fresh	Aged
Composition				
Mg/Al atomic raio	2.5	2.5	2.8	2.8
X-ray diffraction				
a (Å)	3.063	3.065	3.072	3.072
c (Å)	23.361	23.396	23.456	23.421
Crystallite size (Å)	84	106	90	103
^{27}Al MAS-NMR				
δ(ppm)	5.4	5.3	5.5	5.1
FWOTH (Hz)	750	688	833	781
TGA				
T_1 (K)	469	473	464	465
T_2 (K)	678	654	660	658
Weight loss, W_1 (%)	11.7	12.0	10.8	12.4
Weight loss, W_2 (%)	32.6	30.8	28.2	28.1
Net weight loss (%)	44.3	42.8	39.0	40.5
BET measurements				
Surface area (m^2/g)	2.5	94	98	113
Pore volume (cm^3/g)	0.004	0.36	0.68	0.71
Av Pore diameter (Å)	72	153	274	250
Particle size measurements				
$D_{0.5}$ (μ)	207	123	16	20
$D_{0.9}$ (μ)	589	437	34	226
Volume weighed mean (μ)	262	183	20	69

broadening of the peaks wherein broadening is smaller for the samples with better long range ordering, as deduced from FWOTH (full width at one-tenth height) of the peaks, whose values are summarized in Table I. It is clear that IP method (for both fresh and aged samples) showed a smaller line broadening, corroborating PXRD results.

Thermogravimetric analysis of the samples showed a typical two stages mass loss pattern. The first mass loss is due to dehydration of water molecules present in the interlayer while the second mass loss is attributed to simultaneous occurrence of dehydroxylation of sheets and decarbonation of carbonate molecules, with a destruction of layered network. PXRD of the aged samples calcined at 723 K for 6 h (temperature after second transformation) showed reflections for synthetic periclase (MgO) without exhibiting any reflections of hydrotalcite, confirming the decomposition of the layered network. However, the crystallinity of the calcined phase was higher for IP sample compared to COP sample (Fig. 2), similar to fresh samples, suggesting similar degree of topotactic transformation. Further, lattice parameter 'a' calculated by indexing the peaks under cubic system showed values (4.181 Å for MgAl-IP-A and 4.180 Å for MgAl-COP-A) lesser than pure synthetic periclase (4.211 Å) suggesting the dissolution of Al^{3+} in MgO lattice. The TG transformation temperatures (as derived from DTG curves) and mass losses of the samples are given in Table I. No significant difference in transformation temperature was noted between IP and COP samples, in particular for aged, suggesting similar electrostatic interactions between layer and interlayer substantiating PXRD results (similar 'c' parameter). A continuous weight loss was observed up to 973 K for both aged samples, suggesting the presence of strongly held carbonate anions, probably associated with MgAlO solid solutions. *In situ* FT-IR studies for MgAl-COP-A subjected to calcination at various temperatures substantiated this observation exhibiting bands due to carbonate even for the sample calcined at 973 K (Fig. 3). Further, evolved gas analysis of this sample (using quadruple mass spectrometer) showed a small peak for carbon dioxide in the temperature around 923 K corroborating above observations (Fig. 3-inset). No significant difference in the net mass loss was noted with synthesis methodology, although a slightly higher mass loss was noted for IP samples (more so for the weight loss corresponding to second transformation). This could be ascribed for higher aluminum content in IP samples, in turn should possess a higher carbonate content to maintain charge neutrality. TEM of aged samples, given in Fig. 4, indicated a significant difference in the morphology with the variation in synthesis methodology. For MgAl-IP-A, particles were of spherical to platy morphology, however, had a strong tendency to aggregate with each other while a discrete hexagonal morphology was observed for MgAl-COP-A.

Fig. 5 shows N_2 adsorption isotherms of COP and IP aged samples. According to the classification of IUPAC, one can assign these isotherms to type-IV, characteristic of mesopores. Adsorption-desorption profiles showed the presence of hysterisis with the

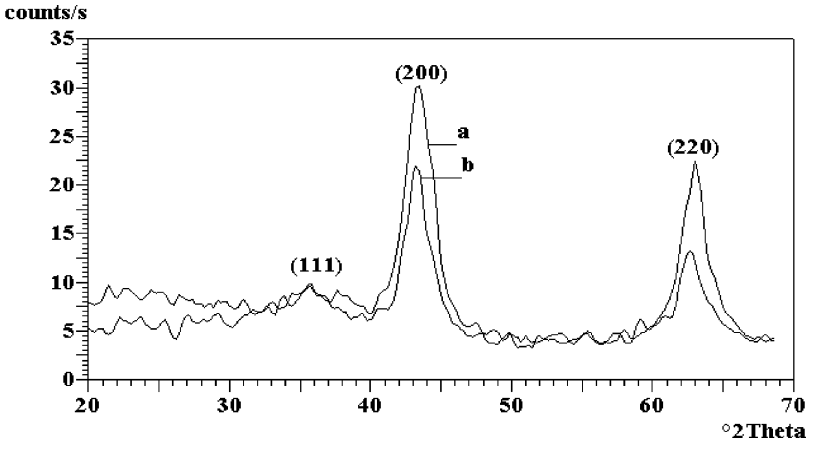

Figure 2 PXRD of (a) MgAl-IP-A and (b) MgAl-COP-A calcined at 723 K for 6 h in air.

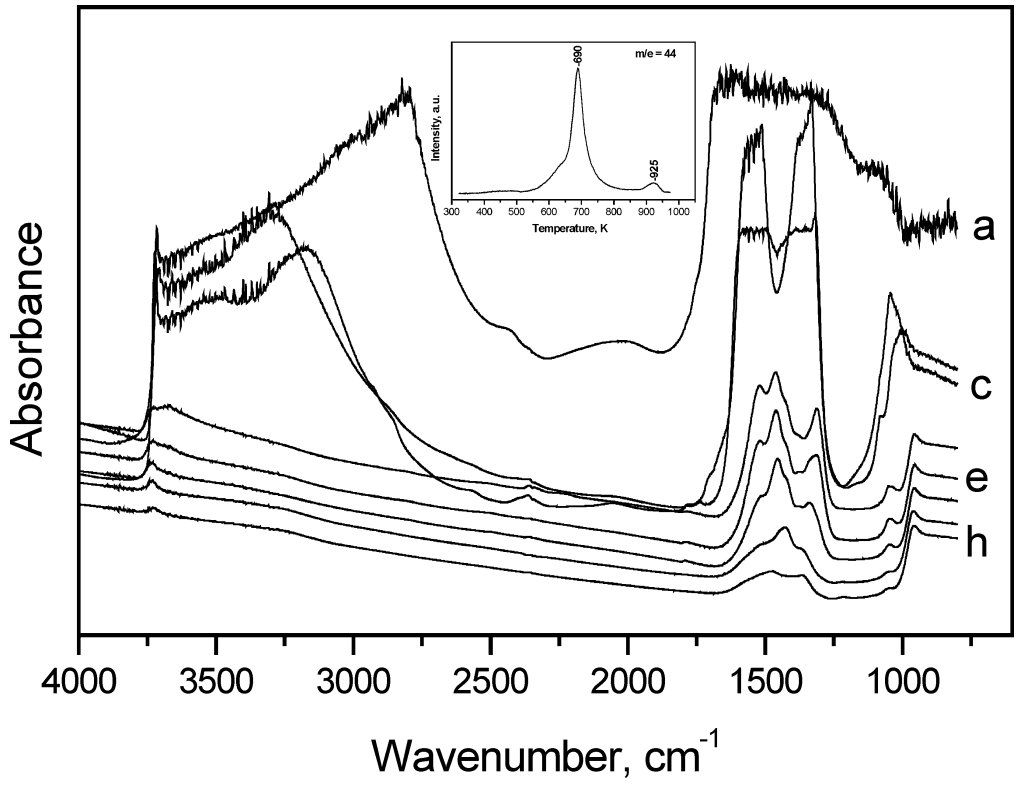

Figure 3 FT-IR study of MgAl-COP-A *in situ* calcined at (a) 303 K, (b) 473 K, (c) 573 K, (d) 673 K, (e) 723 K, (f) 773 K, (g) 873 K and (h) 973 K (inset; QMS—Evolved gas analysis of MgAl-COP-A ($m/e = 44$)).

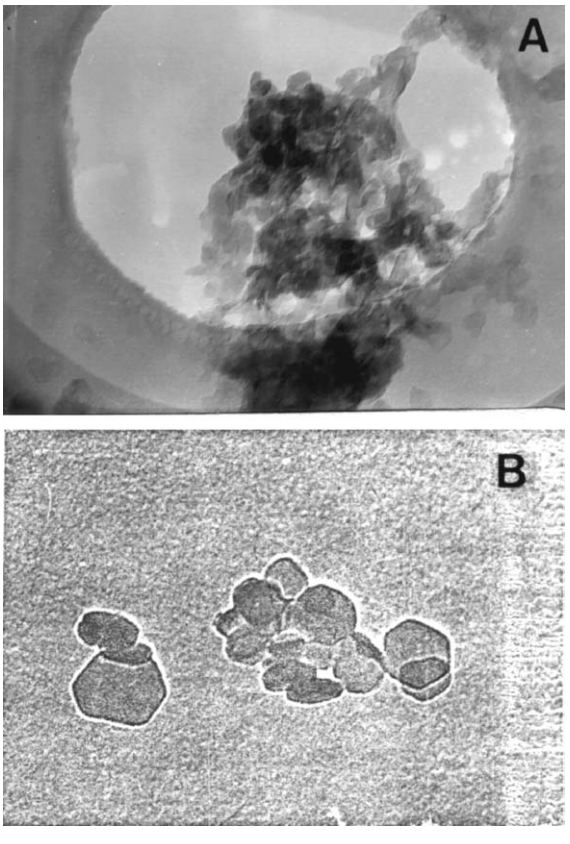

Figure 4 TEM of (a) MgAl-IP-A and (b) MgAl-COP-A (1 mm = 100 Å).

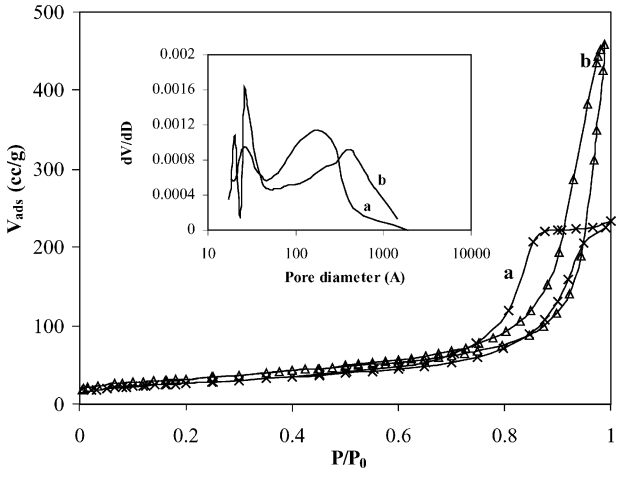

Figure 5 N_2 sorption isotherm of (a) MgAl-IP-A (b) MgAl-COP-A and inset is the corresponding pore size distribution.

loop closing around relative pressure $P/P_0 = 0.5$, however, the shape of hysterisis loop is influenced by the nature of synthesis methodology. No significant difference in the nature of the isotherm was noted between fresh and aged samples synthesized by COP method indicating similar aggregation of particles, while no definite isotherm was exhibited by MgAl-IP-F, which had a poor surface area (2.5 m^2/g), upon aging yielded a type-IV isotherm. It is known, that hysterisis is usually associated with capillary condensation in the mesostructures while the shapes of loops have often been related with the specific pore structures. A closer look at Fig. 4 indicates, that for MgAl-COP-A, desorption started immediately after adsorption is completed (Type-B hysteresis loop) while for MgAl-IP-A, desorption did not occur up to a P/P_0 of 0.88 (Type-A hysteresis loop). This suggests the presence of different pore architecture, in other words, synthesis methodology influences the nature of aggregation of primary particles of these materials. Although attributions of shapes of hysteresis loops

are not well understood, in general, Type-A hysteresis loop is ascribed for pores with narrow necks and wide bodies (often referred as "ink bottle" pores). However, one cannot discard network effects probably associated with the system, wherein desorption from a pore is influenced by the state of neighboring pores, in particular, by the presence of channels connecting pores to the external surface, resulting in pore blocking. For MgAl-COP-A, the hysteresis loop can be explained by considering slit-shaped model, which is generally prevailed for materials having platy morphology (cf. TEM results). In this case, adsorption occur as films on the walls of the slits till pore become completely full of adsorbate and desorption occur through capillary evaporation from the cylindrical menisci. Construction of t-plots showed a straight line with small negative intercept indicating the absence of microporosity. Pore size distributions were constructed employing BJH model and are given in Fig. 4 inset using adsorption branch of the isotherm. Although, both samples exhibited a bimodal distribution, the pore volume and the mean pore radius, summarized in Table I, varied with synthesis methodology. It is clear, that pore volume adsorbed per gram and average pore diameter of the MgAl-COP-A is nearly twice to that of MgAl-IP-A, effectively making a similar surface area (Table I). Further, contribution of macropores was around 35% of the total pore volume for MgAl-COP-A while it was less than 3.5% for MgAl-IP-A, implying the differences in the nature of aggregation of primary particles.

Particle size distribution studies (Fig. 6) showed contrasting results for both fresh as well aged samples and also exhibited variations with the synthesis methodology employed. MgAl-IP-F showed a broad distribution with $d_{0.9}$ (more than 90% of the particles) around 590 μ, which decreased to 437 μ upon aging, indicating deaggreation of particles. However, MgAl-COP-F showed a narrow size distribution with $d_{0.9}$ around 34 μ, upon aging, undergo particle growth exhibited a bimodal distribution with $d_{0.9}$ around 226 μ (Table I). These results clearly enunciate the influence of both synthesis methodology and post treatment in affecting the aggregation and/or agglomeration of the particles wherein agglomeration of fundamental particles is more facilitated in IP methodology compared to COP method (cf. TEM results). Ultrasonication, intended to deagglomerate particles, before the analysis has showed a narrow size profile for MgAl-COP-A with $d_{0.9}$ around 23 μ (without having any contribution from the particles >100 μ) while particle size distribution was not significantly affected for MgAl-IP-A.

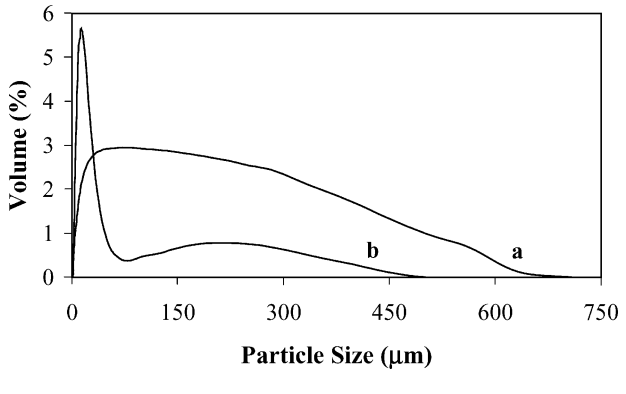

Figure 6 Particle size distribution of (a) MgAl-IP-A and (b) MgAl-COP-A.

The observed differences in the physicochemical properties could be due to the varied local hydrothermal effects associated with the system wherein, a larger heat of neutralization for a shorter time is likely in IP methodology while a smaller amount of heat dissipated for a longer time in COP method. In the case of coprecipitation, synthesis is involved by an addition of both precipitant and metal nitrate occur at different regions in a reactor under turbulent conditions where low supersaturation prevails, subsequently undergo a rapid ionic reaction leading to precipitation. Such an addition results in an uniform macromixing, wherein there will be homogeneity in the local average concentration of all the species. The resulting small particles obtained through primary nucleation will then progressively undergo crystal growth with the thermal energy and supersaturation associated with the system. Such a phenomenon is more facilitated upon aging at elevated temperature where high supersaturation prevails, which essentially controls the frequency of particle sticking and concurrently on crystal growth. However, in the case of instantaneous precipitation, rapid addition of reagents leads to inhomogeneous mixing both at macroscopic and microscopic levels with varied energy dissipation with a stronger local hydrothermal effects, in turn resulting in rapid nonlinear kinetics of primary nucleation and crystal growth (cf. PXRD). Accordingly, gamut of distribution of particles occurs, more so in higher range, where probability of sticking together is lesser, which upon aging lead to breakage of particles. However, the variance in the viscosity of the solution generated (IP method is more than COP method) in influencing the crystal growth cannot be ignored.

4. Conclusions

MgAl-carbonate hydrotalcite was synthesized by two synthesis methodology namely instantaneous precipitation and coprecipitation. PXRD and ^{27}Al MAS-NMR showed that crystallinity of the sample (both fresh and aged) obtained by IP method was higher than the sample prepared through conventional coprecipitation. No significant difference in thermal stability of the materials was noted while TEM showed a variation in the morphology of the particles with the variation in synthesis methodology. Textural studies showed different pore architecture with the variation in synthesis methodology exhibiting varied pore volume and pore size distribution patterns. Contribution of macropores was higher for MgAl-COP-A than for MgAl-IP-A, indicating nature of aggregation of fundamental particles was different with the methodology used. Particle size studies showed a narrow distribution for COP sample while a broad distribution for IP sample. The variations in the crystallinity and growth of the crystals are attributed to variations in local hydrothermal effects, mixing at both microscopic and macroscopic levels and viscosity associated with the system. A detailed

analysis is needed to study the influence of zone of feed addition and stirring speed on crystallinity, number of crystals per unit volume and overall crystallization rate.

Acknowledgements

The author (S.K.) thanks Department of Science and Technology, New Delhi for financial assistance under Young Scientist Scheme. The author also thanks Alexander von Humboldt Foundation for a research fellowship.

References

1. S. KANNAN and R. V. JASRA, *J. Mater. Chem.* **10** (2000) 2311.
2. F. TRIFIRO and A. VACCARI, in "Comprehensive Supramolecular Chemistry, Solid State Supramolecular Chemistry: Two and Three-dimensional Inorganic Networks," edited by J. L. Atwood, J. E. D. Davies, D. D. MacNicol, F. Vogtle, J.-M. Lehn, G. Alberti and T. Bein (Pergamon, Oxford, 1996) Vol. 7, p. 251.
3. F. BASILE, M. CAMPANATI, E. SERWICKA and A. VACCARI (ed.), "Special Issue on Hydrotalcites," *Appl. Clay Sci.* **18** (2001) 1.
4. A. DUBEY, V. RIVES and S. KANNAN, *J. Mol. Catal. General* **181** (2002) 151.
5. B. M. CHOUDARY, M. LAKSHMI KANTAM, V. NEERAJA, K. KOTESWARA RAO, F. FIGUERAS and L. DELMOTTE, *Green Chem.* **3** (2001) 257.
6. S. NARAYANAN and K. KRISHNA, *Appl. Catal.* A **174** (1998) 221.
7. L. M. PARKER, N. B. MILESTONE and R. H. NEWMANN, *Ind. Eng. Chem. Res.* **34** (1995) 1196.
8. V. RIVES and M. A. ULIBARRI, *Coordination Chem. Rev.* **181** (1999) 67.
9. J. C. A. ENGELS, Eur. Patent, 248,492 (1987), to Stamicarbon B.V.
10. H. P. BOEHM, J. STEINLE and C. VIEWEGER, *Angew Chem. Int. Ed. Engl.* **16** (1977) 265.
11. A. DE ROY, C. FORANO, K. EL MALKI and J.-P. BESSE, in "Expanded Clays and Other Microporous Solids," edited by M. L. Occelli and H. E. Robson (Reinhold, New York, 1992) Vol. 2, p. 108.
12. R. M. TAYLOR, *Clay Miner.* **19** (1984) 591.
13. M. A. DREDZON, *Inorg. Chem.* **27** (1988) 4628.
14. H. NIJS, A. CLEARFIELD and E. F. VANSANT, *Microp. Mesop. Mater.* **23** (1998) 97.
15. S. KANNAN, S. VELU, V. RAMKUMAR and C. S. SWAMY, *J. Mater. Sci.* **30** (1995) 1462.
16. S. KANNAN, A. NARAYANAN and C. S. SWAMY, *ibid.* **31** (1996) 2353.
17. S. KANNAN and V. RIVES, *J. Mater. Chem.* **10** (2000) 489.
18. S. KANNAN and C. S. SWAMY, *J. Mater. Sci.* **32** (1997) 1623.

Received 3 December 2003
and accepted 3 June 2004